

# High-Resolution $T_1$ and $T_2$ Mapping of the Brain in a Clinically Acceptable Time with DESPOT1 and DESPOT2

Sean C. L. Deoni,<sup>1,2</sup> Terry M. Peters,<sup>1,2,3</sup> and Brian K. Rutt<sup>1,2,3\*</sup>

Variations in the intrinsic  $T_1$  and  $T_2$  relaxation times have been implicated in numerous neurologic conditions. Unfortunately, the low resolution and long imaging time associated with conventional methods have prevented  $T_1$  and  $T_2$  mapping from becoming part of routine clinical evaluation. In this study, the clinical applicability of the DESPOT1 and DESPOT2 imaging methods for high-resolution, whole-brain,  $T_1$  and  $T_2$  mapping was investigated. In vivo, 1-mm<sup>3</sup> isotropic whole-brain  $T_1$  and  $T_2$  maps of six healthy volunteers were acquired at 1.5 T with an imaging time of <17 min each. Isotropic maps (0.34 mm<sup>3</sup>) of one volunteer were also acquired (time <21 min). Average signal-to-noise within the 1-mm<sup>3</sup>  $T_1$  and  $T_2$  maps was ~20 and ~14, respectively, with average repeatability standard deviations of 46.7 ms and 6.7 ms. These results demonstrate the clinical feasibility of the methods in the study of neurologic disease. *Magn Reson Med* 53:237–241, 2005. © 2004 Wiley-Liss, Inc.

**Key words:**  $T_1$  mapping;  $T_2$  mapping; fast imaging; human brain imaging

## INTRODUCTION

Previous studies examining the utility of voxelwise determination, or “mapping,” of the longitudinal and/or transverse ( $T_1$  and  $T_2$ ) relaxation times in the context of neurologic disease have demonstrated variations in  $T_1$  and  $T_2$  within specific brain regions within autism (1), schizophrenia (2), epilepsy (3), Parkinson’s (4), multiple sclerosis (5), and a host of other disorders. Despite the demonstrated value, volumetric  $T_1$  and  $T_2$  mapping is not part of routine clinical assessment, likely owing to the low resolution and exhaustive scan times associated with conventional mapping methods. A further limitation of the noted studies is that comparisons between patient and control groups have been limited to mean values of gross anatomic regions (i.e., frontal region white matter, the caudate nucleus, thalamus, etc.). Averaging values over these large regions masks localized  $T_1$  and  $T_2$  changes within these structures, hindering our ability to study disease pathogenesis at high levels of detail.

The ability to accurately and precisely map  $T_1$  and  $T_2$  at high resolution (less than 1-mm<sup>3</sup> isotropic voxels) over large volumes would allow more thorough investigations of relaxation time changes in disease states. Unfortunately, current conventional and accelerated mapping methods (6–9) do not allow for such high-resolution scanning in a clinically practical time frame (<30 min). We have recently developed a set of rapid combined  $T_1$  and  $T_2$  mapping approaches (10), referred to as DESPOT1 and DESPOT2 (driven equilibrium single pulse observation of  $T_1$  and  $T_2$ , respectively). With DESPOT1,  $T_1$  is calculated from a series of spoiled gradient recalled-echo (SPGR) images acquired over a range of flip angles with constant repetition time (TR). The SPGR signal equation can be written in a linear form,  $SI_{SPGR}/\sin\alpha = SI_{SPGR}/\tan\alpha \times E_1 + M_o(1 - E_1)$ , where  $SI_{SPGR}$  is the SPGR signal intensity associated with flip angle  $\alpha$ ,  $M_o$  is a factor proportional to the equilibrium longitudinal magnetization, and  $E_1 = \exp(-TR/T_1)$ . Plotting  $SI_{SPGR}/\sin\alpha$  versus  $SI_{SPGR}/\tan\alpha$  allows  $T_1$  to be calculated from the slope of this line as  $T_1 = -TR/\ln(\text{slope})$ .

In DESPOT2,  $T_2$  is calculated from a series of fully balanced steady-state free precession (SSFP) images also acquired over a range of  $\alpha$  with constant TR. As with the SPGR signal equation, the SSFP signal equation can be written in a linear form as  $SI_{SSFP}/\sin\alpha = SI_{SSFP}/\tan\alpha \times (E_1 - E_2/1 - E_1E_2) + M_o(1 - E_1)E_2/(1 - E_1E_2)$ , where  $SI_{SSFP}$  is the SSFP signal intensity associated with flip angle  $\alpha$  and  $E_2 = \exp(-TR/T_2)$ . Plotting  $SI_{SSFP}/\sin\alpha$  versus  $SI_{SSFP}/\tan\alpha$ , and making use of the  $T_1$  information obtained previously with DESPOT1, allows calculation of  $T_2$  as  $T_2 = -TR/\ln[(\text{slope} - E_1)/(\text{slope} \times E_1 - 1)]$ .

The linearization property of the SPGR and SSFP signal equations permits rapid acquisition (because only two flip angles are required to calculate each of  $T_1$  and  $T_2$ ) as well as efficient postprocessing. Comparing the efficiency (defined as signal-to-noise ratio of the calculated  $T_1$  or  $T_2$  map per unit scan time) of the DESPOT methods with alternative mapping strategies, shows DESPOT1 and DESPOT2 to be up to 3 times more efficient than multipoint inversion-recovery and spin-echo methods (10). This high efficiency makes DESPOT1 and DESPOT2 ideal for performing high-resolution comparative relaxation time studies between normal and patient groups.

In this article we demonstrate the utility of DESPOT1 and DESPOT2 for high-resolution  $T_1$  and  $T_2$  mapping of the brain and present the first matched whole-brain and deep brain  $T_1$  and  $T_2$  maps with 1-mm<sup>3</sup> and 0.34-mm<sup>3</sup> isotropic resolution, respectively. From these high-resolution maps, we demonstrate improved contrast within the deep brain and thalamus compared with traditional  $T_1$ -weighted images. These results illustrate the potential of the DESPOT methods in the study of neurologic disease and highlight the advantages of quantitative imaging for

<sup>1</sup>Imaging Research Laboratories, Robarts Research Institute, London, Ontario, Canada

<sup>2</sup>Department of Medical Biophysics, University of Western Ontario, London, Ontario, Canada

<sup>3</sup>Department of Diagnostic Radiology and Nuclear Medicine, University of Western Ontario, London, Ontario, Canada

Grant sponsor: Canadian Institutes for Health Research; Grant number: MT-11540 and GR-14973; Grant sponsor: Canadian Foundation for Innovation; Grant sponsor: University of Western Ontario; Grant sponsor: General Electric Medical Systems.

Correspondence to: Brian K. Rutt, Imaging Research Laboratories, Robarts Research Institute, Post Office. 5015, 100 Perth Drive, London, Ontario, Canada N6A 5K8. E-mail: brutt@imaging.robarts.ca

Received 17 February 2004; revised 19 August 2004; accepted 20 August 2004

DOI 10.1002/mrm.20314

Published online in Wiley InterScience (www.interscience.wiley.com).

© 2004 Wiley-Liss, Inc.

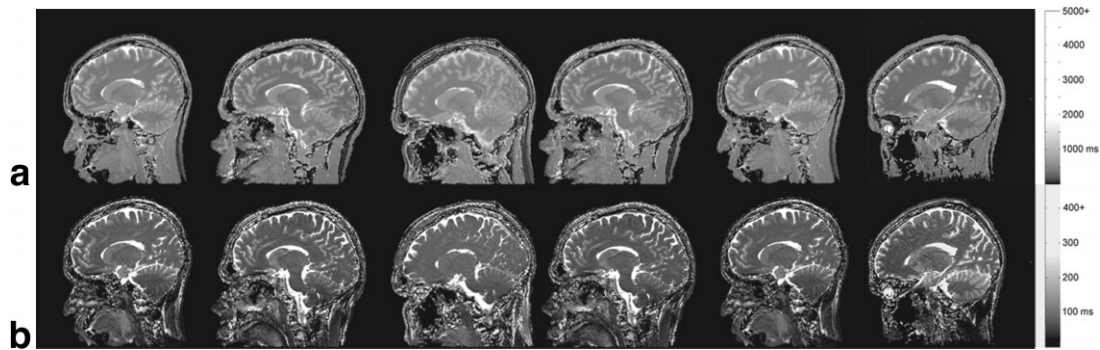


FIG. 1. Representative sagittal slices (at approximately the same location) through the whole brain, 3D (a)  $T_1$  and (b)  $T_2$  map volumes for each of the six volunteers.

improving image contrast compared with traditional image acquisition methods.

## METHODS

All imaging experiments for this study were performed using a GE CV/i 1.5-T scanner with an eight-channel head coil. Informed consent was obtained prior to scanning and the study was performed with approval from the Ethics Review Board at the University of Western Ontario.

To demonstrate the clinical utility of DESPOT1 and DESPOT2, sagittally oriented whole-brain  $T_1$  and  $T_2$  maps were acquired of six volunteers with the following imaging parameters: DESPOT1: Matrix:  $256 \times 256 \times 128$ , field of view (FOV):  $25 \text{ cm} \times 25 \text{ cm}$ , slab thickness (ST) of 13 cm, flip angles (FA):  $4^\circ$  and  $15^\circ$ , repetition time (TR): 11.7 ms, echo time (TE): 2.4 ms, bandwidth (BW):  $\pm 15.6 \text{ kHz}$  and imaging time for both flip angles ( $T_{\text{imag}}$ ): 12:46. DESPOT2: Matrix:  $256 \times 256 \times 128$ , FOV:  $25 \text{ cm} \times 25 \text{ cm}$ , ST = 13 cm, FA:  $15^\circ$  and  $55^\circ$ , TR: 3.7, TE: 1.8, BW:  $\pm 62.5.0 \text{ kHz}$  and  $T_{\text{imag}}$ : 4:02. Combined imaging time for both maps was therefore 16 min and 48 s.

To limit patient motion between acquisitions, head fixation via a chinstrap in combination with foam padding was used. To reduce artifacts associated with swallowing and eye movement, the volunteers were asked to refrain

from swallowing and to keep their eyes closed during each of the four scans.

In addition to these whole-brain maps, ultra-high-resolution DESPOT1 and DESPOT2  $T_1$  and  $T_2$  maps were acquired of the deep brain region (i.e., the thalamus, basal ganglia, globus pallidus, and putamen). These structures are primary targets for the surgical treatment for a variety of functional disorders, and given their anatomic complexity, an isotropic spatial resolution of better than  $1 \text{ mm}^3$  is desirable for imaging these regions. To test the application of the DESPOT methods in this area, axially oriented data were acquired of one volunteer with  $0.34\text{-mm}^3$  isotropic resolution with the following parameters: DESPOT1: Matrix:  $256 \times 256 \times 128$ , FOV:  $18 \text{ cm} \times 18 \text{ cm}$ , ST = 9 cm, FA:  $5^\circ$  and  $15^\circ$ , TR: 13.4 ms, TE: 2.9 ms, BW:  $\pm 7.81 \text{ kHz}$  and  $T_{\text{imag}}$ : 14:44. DESPOT2: Matrix:  $256 \times 256 \times 128$ , FOV:  $18 \text{ cm} \times 18 \text{ cm}$ , ST = 9 cm, FA:  $15^\circ$  and  $60^\circ$ , TR: 5.6 ms, TE: 2.8 ms, BW:  $\pm 125.0 \text{ kHz}$  and  $T_{\text{imag}}$ : 6:07. Ten  $T_1$  and  $T_2$  maps were acquired over a period of 4 days and the calculated maps were subsequently linearly coregistered (11) and averaged. Total time for the 10  $T_1$  and  $T_2$  maps was approximately 3.5 h.

## RESULTS

Figures 1 and 2 show representative sagittal and axial slices through the whole-brain  $T_1$  and  $T_2$  maps of each of

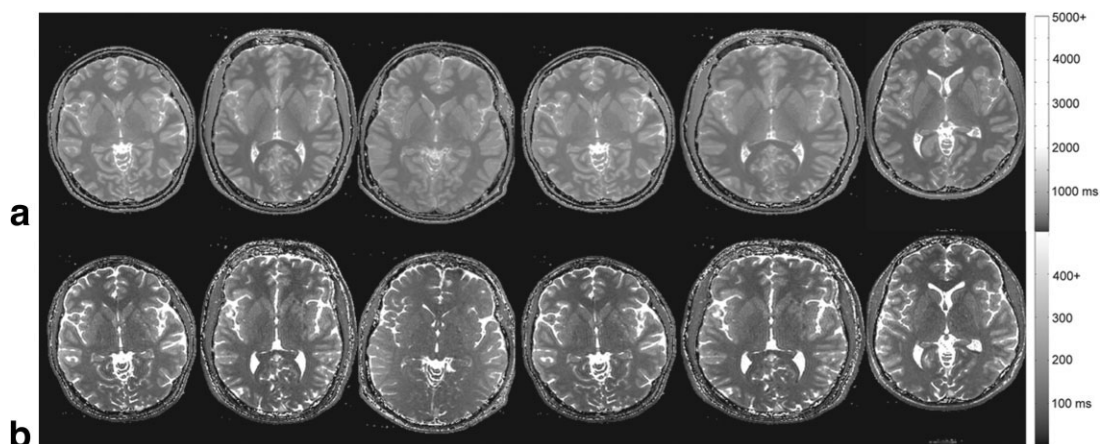


FIG. 2. Representative axial slices (at approximately the same location) through the whole brain, 3D (a)  $T_1$  and (b)  $T_2$  map volumes for each of the six volunteers.

Table 1  
Mean  $T_1$  and  $T_2$  Values Obtained from the Six High-Resolution, Whole-Brain  $T_1$  and  $T_2$  Maps

Brain tissue	$T_1$ (ms)	$T_2$ (ms)
White matter	608 (23)	54 (4)
Gray matter	1065 (51)	98 (7)
Caudate nucleus	1064 (56)	89 (6)
Hippocampus	1183 (57)	92 (8)
Amygdala	1093 (56)	103 (10)
Pons	783 (37)	64 (5)

Note. Both the mean and standard deviation values (shown in parentheses) were calculated from data obtained from regions of interest placed in each of the six volunteers and pooled together.

the six volunteers and demonstrate the high map quality achievable with the DESPOT methods. Average SNR in the  $T_1$  and  $T_2$  maps (calculated from regions of interest placed within frontal white matter) of 19.6 and 13.7, respectively, with repeatability (defined as SD in these  $T_1$  and  $T_2$  values computed using pooled data obtained from anatomically matched regions in all six volunteers) of 46.7 ms and 6.7 ms, respectively.

Mean  $T_1$  and  $T_2$  values (and corresponding standard deviations) of a variety of brain tissues or regions obtained from regions of interest (40–50 voxels) placed within the calculated maps are shown in Table 1. The mean and SD values quoted in Table 1 were calculated from the pooled data from all six individuals (i.e., data obtained from regions of interest placed within white matter in the six maps were pooled and the mean and SD calculated from this pooled data). Values given for white and gray matter and the caudate nucleus agree well with those reported in literature (12) with an average absolute difference between mean values of 5%.  $T_1$  and  $T_2$  values of the hippocampus, amygdala, and the pons at 1.5 T have not been previously published to the best of our knowledge. Our results further illustrate the high accuracy and precision afforded by the DESPOT methods. With a combined acquisition time of less than 17 min for maps of the entire brain, additional averages could easily be acquired without making the study time excessively long, permitting further increases in image quality and estimate precision.

The ability to perform ultra-high-resolution imaging with DESPOT1 and DESPOT2 is shown in Fig. 3 by representative slices through a 0.34-mm<sup>3</sup> isotropic  $T_1$  and  $T_2$  map of the deep brain. Average SNR within the averaged  $T_1$  and  $T_2$  maps are 26.3 and 16.2, respectively. Within the

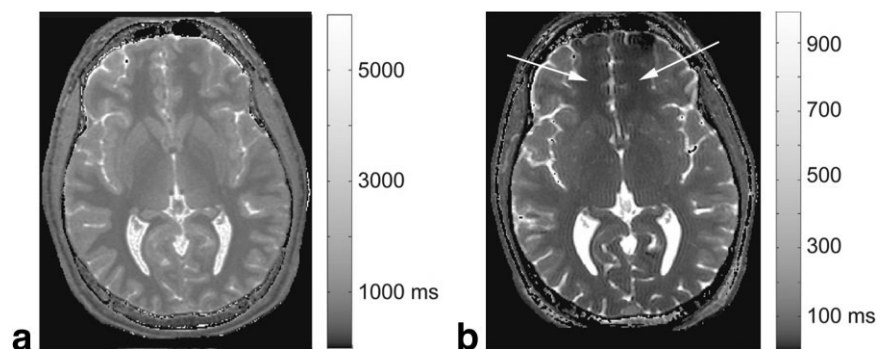
$T_2$  map, areas of low or no signal, resulting from the SSFP off-resonance banding artifact (13), are noticeable at the air–tissue interfaces, particularly within the frontal lobe region as shown by the arrows. Examining the  $T_1$  map in greater detail, a series of matched coronal slices [anterior (i) to posterior (iii)] through the thalamus from the 10× averaged  $T_1$ -weighted image (corresponding to the SPGR image acquired at 15°) and the  $T_1$  map of the deep brain are shown in Fig. 4 a and b. In this figure, we have inverted the gray-scale of the parametric  $T_1$  map so that the contrast is similar to that of the  $T_1$ -weighted image. From this series of images increased contrast is seen in the map images compared with the standard  $T_1$ -weighted images and that structural differences are evident in the  $T_1$  maps that are not distinguishable in the weighted images, despite the higher SNR of the latter. This result suggests that subtle  $T_1$  differences may exist throughout the thalamus that are masked in the  $T_1$ -weighted images due to the influence of proton density and  $T_2$  effects. Both of these corrupting influences are cleanly removed within the pure  $T_1$  map.

## DISCUSSION AND CONCLUSIONS

The value of quantitative imaging in the study and diagnosis of neurologic disease has been well established. Unfortunately, the lack of a rapid, accurate, and precise method for volumetric  $T_1$  and  $T_2$  mapping has hindered the clinical adoption of quantitative imaging. Further, the lack of such a method has limited our ability to more thoroughly study changes in these values in pathology at fine levels of detail. The aim of this study was to demonstrate DESPOT1 and DESPOT2 as a method for repeatable, rapid, clinically feasible, high-resolution, whole-brain combined  $T_1$  and  $T_2$  mapping.

The high-resolution and large volumetric coverage afforded by DESPOT1 and DESPOT2 allows more thorough characterization of tissues and structures of interest as well as investigation of changes in  $T_1$  and  $T_2$  in anatomically connected by structurally separated areas. Such targeted (subregional) comparisons of  $T_1$  and  $T_2$  between patient and control groups have not been previously possible. Further, the acquisition of “pure”  $T_1$  and  $T_2$  maps may yield increased contrast within brain structures, such as between the major nuclei of the thalamus. The advantage of acquiring pure  $T_1$  and  $T_2$  maps over more traditional  $T_1$ - and  $T_2$ -weighted images is that the confounding influence of  $T_2$ - on the  $T_1$ -weighted signal (and vice versa)

FIG. 3. Representative axial slices through the 10× averaged 0.34-mm<sup>3</sup> isotropic deep brain (a)  $T_1$  and (b)  $T_2$  maps. Arrows indicate areas of signal void resulting from the SSFP banding artifact.



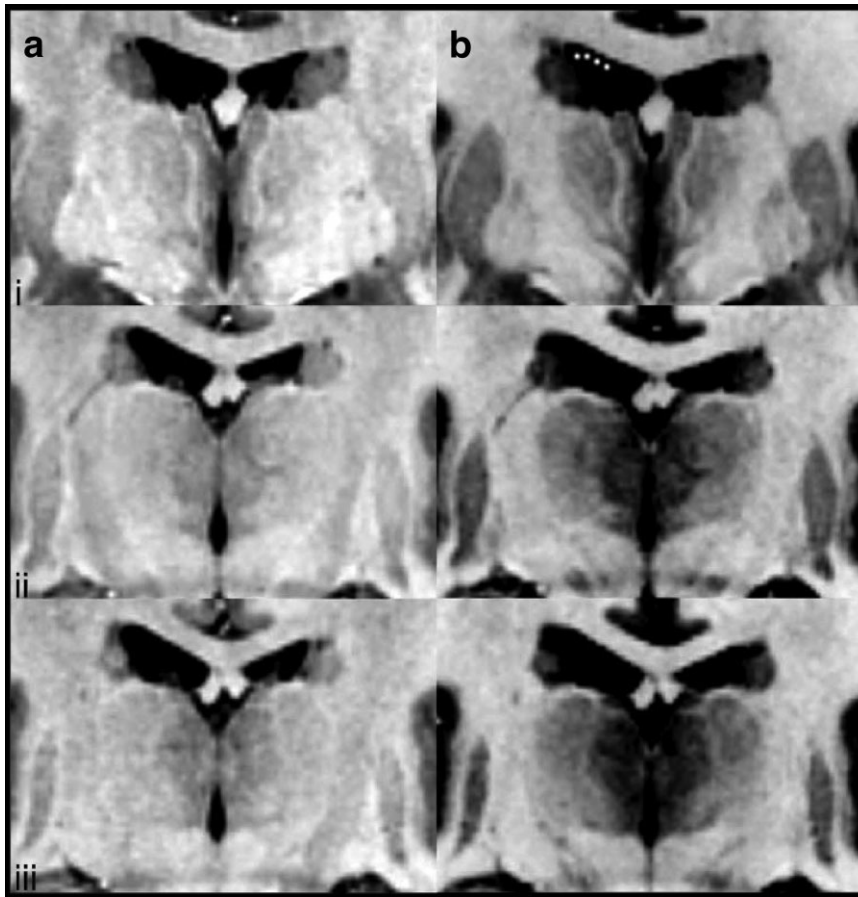


FIG. 4. Comparison of coronal slices through the thalamus from the (a) 10 $\times$  averaged deep brain  $T_1$ -weighted image and (b) the 10 $\times$  averaged deep brain  $T_1$  map. Slices move from anterior (i) to posterior (iii). Enhanced contrast is seen in the map image compared with the  $T_1$ -weighted images. The grayscale of the parametric images have been inverted to better match the contrast seen in the  $T_1$ -weighted images.

is eliminated. The influence of proton density and coil sensitivity on the image contrast is also removed because the mapping process separates these two effects cleanly.

Some potential objections and limitations of the DESPOT2 method include the influence of  $B_1$  inhomogeneities on the  $T_1$  and  $T_2$  estimates, artifacts due to off-resonance ( $B_0$  inhomogeneities) in SSFP (DESPOT2), and the assumption of monoexponential  $T_2$  relaxation.

A dominant source of error in both the  $T_1$  and  $T_2$  estimates is imprecise knowledge of the flip angle used. The use of optimized RF pulses [i.e., SLR pulses (14)], and the 3D nature of the sequences reduce the severity of these errors, particularly within the center portion of the volume. Patient-induced  $B_1$  inhomogeneities, which are more difficult to correct, do not appear to play a significant role at 1.5 T given the uniform intensity across the maps. These effects, however, are anticipated to increase with increased field strength, in which case quantitative  $B_1$  mapping could be performed to calibrate the flip angle  $\alpha$  as a function of spatial location throughout the volume of interest, or  $B_1$  insensitive pulses could be employed. Simulations investigating  $T_1$  accuracy as  $\alpha$  was varied from 50% to 150% of the prescribed value, demonstrated that the results were highly sensitive to imprecision in  $\alpha$ , with a  $T_1$  estimate inaccuracy >10% with a 5% deviation in  $\alpha$ . Similar results were found for  $T_2$ .

The SSFP banding artifact, particularly noticeable near the sinuses, inner ear and other regions of large susceptibility differences, present as bands of signal hypo-inten-

sity. A common method of reducing the appearance of these artifacts within the imaged volume is to minimize TR (12). With current gradient hardware capabilities, TRs less than 4.5 ms are possible even at the high resolution that we demand, which greatly diminishes the appearance of these artifacts. Investigation of off-resonance effects on calculated  $T_2$  estimates via simulations have shown good estimate accuracy (less than 8% deviation with phase offsets of up to  $\pm 30^\circ$ ). With appropriate shimming, a root mean square homogeneity of  $\pm 8$  Hz can be achieved across the deep brain, corresponding to a phase offset of less than 10 degrees with a TR of 5 ms. The method is therefore expected to perform well throughout most of the brain.

In areas where greater off-resonance conditions exist (i.e., near the sinuses), phase-cycled DESPOT2 (15) may be used to significantly reduce the appearance of these artifacts. In this approach two or more sets of SSFP data are collected with different phase cycling patterns along the RF pulse train. This phase cycling acts to shift the bands to different locations within each SSFP image.  $T_2$  maps are calculated from each data set and combined using a weighted averaging approach. Although banding is noticeable in the 0.34-mm<sup>3</sup> isotropic images presented in Fig. 3, the bands were very localized to the sinus region and do not detract from the information contained in the  $T_2$  maps of the deep brain region.

Although recent in vitro, in vivo, and postmortem studies (16,17) have demonstrated a biexponential  $T_2$  behavior within white matter (attributed to water within and sur-

rounding the myelin layers of neuronal fibers), prior  $T_1$  and  $T_2$  studies of neurologic disease have focused exclusively on single  $T_1$  and  $T_2$  relaxation time measurements. Thus, although it is possible to include multiexponential behavior into the DESPOT2 (and DESPOT1) framework, the clinical utility of measuring the short  $T_2$  component in white matter in neurologic disorders (apart from multiple sclerosis) has yet to be established.

The presented DESPOT1 and DESPOT2 methods allow the acquisition of large matrix ( $256 \times 256 \times 128$ ) high-resolution ( $1\text{-mm}^3$ )  $T_1$  and  $T_2$  maps with high precision and SNR in under 17 min at 1.5 T, making whole-brain mapping clinically feasible for the first time. The methods also permit acquisition of  $0.34\text{-mm}^3$  isotropic resolution maps of the deep brain, though with significantly reduced SNR. The contrast observed within these higher resolution maps suggest their utility in surgical planning of functional stereotactic procedures; however, with a cumulative imaging time of 3.5 h, such imaging is not yet clinically practical. The development of dedicated, multichannel head coils and the move to higher field strength, however, may provide the SNR gains necessary to bring this scan time down to clinically realistic levels.

The ability to acquire high-resolution, quantitative images over the whole brain provides a more complete characterization of the various brain regions and therefore has tremendous potential for the study, understanding, and monitoring of disease processes.

## ACKNOWLEDGMENTS

Thanks are extended to Adrian Koziak, Melanie Josseau, and Kathleen Surry for their assistance in data collection. BKR receives salary support from the Barnett-Ivey Heart and Stroke Foundation of Ontario Endowed Chair award.

## REFERENCES

- Friedman SD, Shaw DW, Artru AA, Richards TL, Gardner J, Dawson G, Posse S, Dager SR. Regional brain chemical alterations in young children with autism spectrum disorder. *Neurology* 2003;60:100–107.
- Williamson P, Pelz D, Merskey H, Morrison S, Karlik S, Drost D, Carr T, Conlon P. Frontal, temporal and striatal proton relaxation times in schizophrenic patients and normal comparison subjects. *Am J Psych* 1992;149:549–551.
- Pitkamen A, Laakso M, Kalviainen R, Vairio P, Lehtovirta M, Riekkinen P, Soininen H. Severity of hippocampal atrophy correlates with the prolongation of MRI T2 relaxation time in temporal lobe epilepsy but not in Alzheimer's disease. *Neurology* 1996;46:1720–1730.
- Bartozokis G, Sultzer D, Cummings J, Holt LE, Hance DB, Henderson VW, Mintz J. In-vivo evaluation of brain iron in Alzheimer disease using magnetic resonance imaging. *Arch Gen Psych* 2000;57:47–53.
- Larsson HB, Frederiksen J, Petersen J, Nordenbo A, Zeeberg I, Henriksen O, Olesen J. Assessment of demyelination, edema and gliosis by in-vivo determination of T1 and T2 in the brain of patients with acute attack of Multiple Sclerosis. *Magn Reson Med* 1989;11:337–348.
- Brix G, Schad LR, Deimling M, Lorenz WJ. Fast and precise T1 imaging using a TOMROP sequence. *Magn Reson Imag* 1990;8:351–256.
- Bluml S, Schad LR, Boris S, Lorenz WJ. Spin-lattice relaxation time measurement by means of a TurboFLASH technique. *Magn Reson Med* 1993;30:289–295.
- Deichmann R, Adolf H, Noth U, Morrissey S, Schwarzbauer C, Haase A. Fast T1 mapping with SNAPSHOT-FLASH imaging. *Magn Reson Imag* 1995;13:633–639.
- McKenzie CA, Chen Z, Drost DJ, Prato FS. Fast acquisition of quantitative T2 maps. *Magn Reson Med* 1999;41:208–212.
- Deoni SCL, Rutt BK, Peters TM. Rapid combined T1 and T2 mapping using gradient recalled acquisition in the steady state. *Magn Reson Med* 2003;49:515–526.
- Collins DL, Neelin P, Peters TM, Evans AC. Automatic 3D intersubject registration of MR volumetric data in standardized Talairach space. *J Comput Assist Tomogr* 1994;18:192–205.
- Breger RK, Rimm AA, Fisher ME, Papke RA, Houghton VM. T1 and T2 measurements on a 1.5T commercial MR imager. *Radiology* 1989;171:282–276.
- Zur Y, Stokar S, Bendel P. An analysis of fast imaging sequences with steady state transverse magnetization refocusing. *Magn Reson Med* 1988;6:175–193.
- Pauly P, Le Roux P, Nishimura D, Macovski A. Parameter relations for the Shinnar–Le Roux selective excitation pulse design algorithm. *IEEE TMI* 1991;10:53–65.
- Deoni SCL, Ward HA, Peters TM, Rutt BK. Rapid T2 estimation with phase-cycled variable nutation steady-state free precession. *Magn Reson Med* In Press.
- MacKay A, Whittal K, Adler J, Li D, Paty D, Graeb D. In-Vivo visualization of myelin water in brain by magnetic resonance. *Magn Reson Med* 1994;31:673–677.
- Does MD, Snyder RE. T2 relaxation in peripheral nerve measured in vivo. *Magn Reson Imag* 1995;13:575–580.